École Centrale de Nantes

Tensegrity analysis - Horizontal orientation stability

By Raghuveer Siddaraboina

Supervised by
Professor Swaminath Venkateswaran and Professor Damien Chablat

Contents

List of figures

Introduction

A bio-inspired piping inspection robot was designed and developed at LS2N,France. This robot accomplishes the locomotion of a caterpillar in six steps to move inside a pipeline. However, the prototype is a rigid model which restricts its application to straight pipelines. By the addition of articulation units, the robot can be made reconfigurable. Some interesting researches on piping inspection robots that pass through pipe bends include i) The robot of Chen et al. Where double hook joint is employed, ii) THES-I robot of Hirose and al. Where a universal joint actuated by DC-motor is used and iii) Robot of Brunete and al, that uses SMA spring with microcontrollers. Most of these researches have articulation units either in passive mode or active mode but not a combination of both. By analyzing key design issues namely passive compliance, active compliance and tilt limits, a tensegrity mechanism that uses a passive universal joint and three tension springs was proposed as a solution for the bio-inspired robot of LS2N.This mechanism can work passively when the robot passes through a pipe bend at $\pi/2$ radians. In the event of a T-union or junction, cable actuation can be performed on the tensegrity mechanism to follow a given path.

A Tensegrity analysis in Horizontal orientation is performed on the structure in order to determine its stability with zero applied forces and with a preload. A tensegrity structure is said to be stable when the resultant moments are zero and also when the second order derivative of the total potential energy i.e, K_α is positive.

Bibliography

In industries such as nuclear, chemical and sewage, it is difficult for a human being to perform inspection or interventions. Manual intervention could not only lead to long-term radiation effects but also pose a serious threat to human life. Piping inspection robots play an essential role in such scenarios as they reduce human effort and impose lesser risks to life. Generally, the locomotion principles of these robots can employ mechanical systems or can be inspired from animals. Kassim et al proposed a distinction between these two categories where the mechanical systems can use wheels and pulleys, telescopic system, impact modules or natural peristalsis to accomplish the locomotion. On the other hand, the bio-inspired systems can mimic their locomotions from animals such as earthworms, snakes, millipedes, lizards or an octopus. Presently, several piping inspection robots have been developed. Nayak et al proposed a screw type robot that is capable of working inside 127–152 mm diameter pipelines. Zhang et al developed a flexible inchworm type robot that can adapt itself to varying diameters of pipes. Kwon et al developed an inspection robot that employs a caterpillar module with four bar linkages to work inside 100 mm diameter pipelines with bends and junctions. However, the design and development of inspection robots for pipelines less than 100 mm diameter is a big challenge. In addition, these piping inspection robots encounter some key problems, which include: (i) movement of the robot inside straight or curved sections of pipe while towing a payload; (ii) accurate positioning of the robot on the zone to be intervened; (iii) effective

communication between onboard sensors and central station; and (iv) performing the desired mechanical activity such as drilling by withstanding the load of the mounted device.

Initial design

The locomotion principle of the robot is inspired from a caterpillar. The motion of a caterpillar is subdivided into three modules: a central blocking module and two elongation modules with one at the front and the other at the rear. A classical way to mimic this locomotion can be accomplished with the help of pneumatic bellows for blocking and electric motors for elongation. However, while moving inside nuclear power plant pipelines there exists dust particles which limits the use of pneumatic systems. Hence, electrical actuators are used in the robot. A comparative study by Henry et al proposes a mechanism that is capable of simulating the locomotion of a caterpillar which is mimicked by using three electrical actuators. A cross-sectional view of the robot inside a pipeline of radius r is represented in Figure

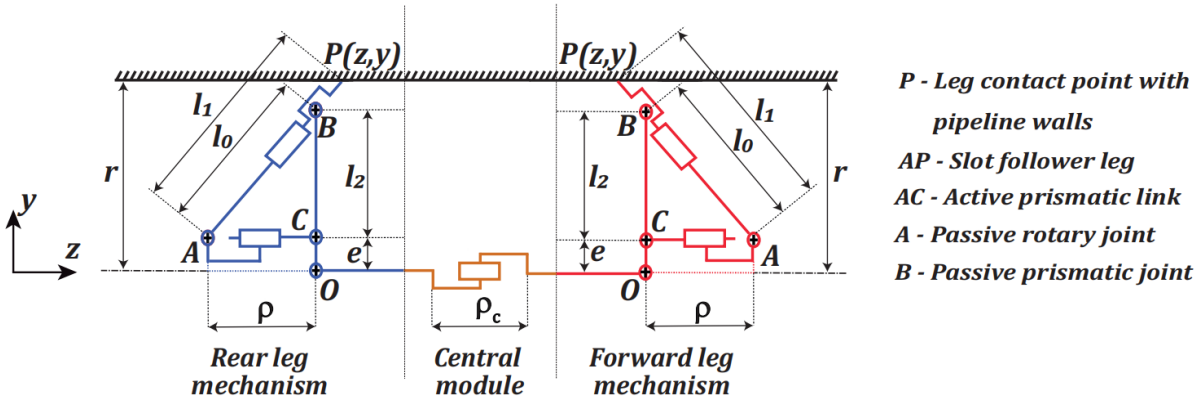

Figure 1 : Cross section view of the robot representing the actuators and leg mechanisms inside a pipeline of radius r

Architecture of the new piping inspection robot

In order to address the compliance factors and tilt limits, a new architecture of the bio-inspired robot has been proposed and it is represented in Figure. The caterpillar locomotion from has been retained in this architecture. This module ensures tight contact with pipeline walls through a force control algorithm inside vertical and horizontal orientations. By the introduction of suitable articulation units between each motor modules, the robot can be made to pass through pipe bends. While moving through bends, the entire robot resembles an “Elephant trunk” wherein the force is transmitted from the front to rear module to pull the robot in order to pass through the curvature and vice-versa. The articulation units are designed with a view that they undergo deflection like a beam without torsion

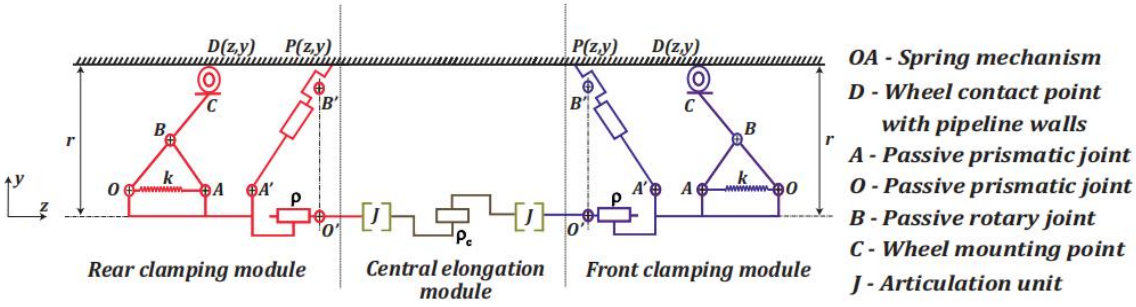

Figure 2 : Cross section view of the new bio-inspired robot inside a pipeline of radius r

Design of a tensegrity mechanism

A tensegrity type mechanism is proposed to be introduced between the motor modules which can facilitate the robot to pass through 90-degree bends or junctions by bending up to a certain angle. In the existing design of the robot, the motor units were coupled rigidly. Between each unit, a universal joint and three tension springs are introduced. The universal joint remains passive and the issue of passive compliance could be addressed by this joint and springs for a 90-degree pipe bend. For active compliance, cables will be introduced that can pass through the springs. From a central control unit, the cables can be actuated and the robot can be made to move or bend along a fixed direction while encountering a junction.

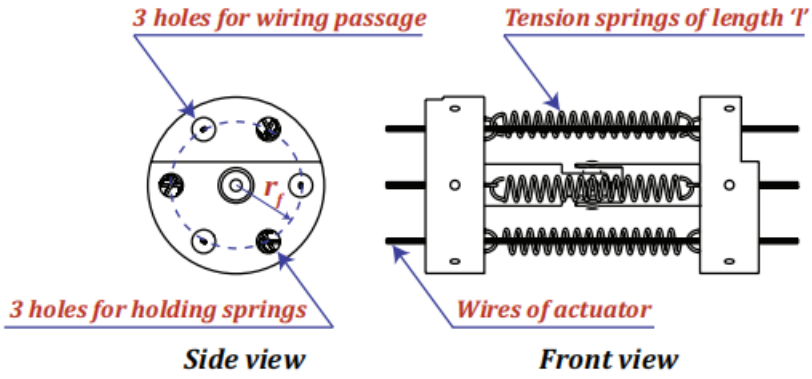

Figure 3 : Proposed tensigrity structure with three springs and a universal joint

The proposed tensegrity mechanism is represented below:

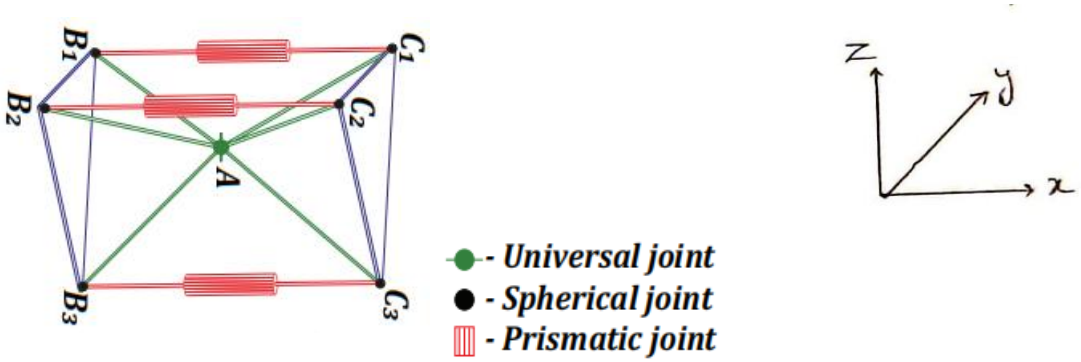

Figure 4 :3-d line diagram of the mechanism

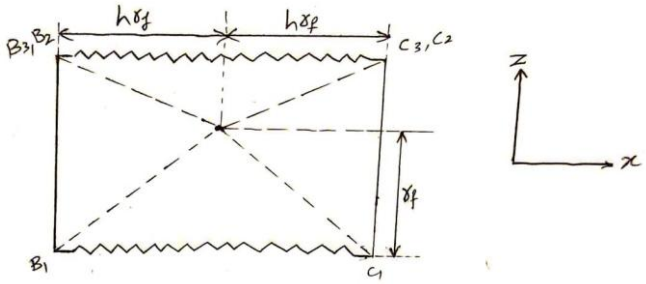

Figure 5 :2-d line diagram of the mechanism

The flanges used for spring mounting is carried over from the existing prototype. The three springs are mounted at an angle of 120 degrees between each other. Three tension springs are used because they ensure stability of the system as well as the bending limit of the universal joint is controlled when the robot works through 3D pipe profiles. Three cables for actuation of the system passes through the springs. The other three holes on the flange can be used for routing the wires coming out from the motors used in the caterpillar module. The springs are mounted at radius r_f from the central axis of the flange. Using CATIA software, a 3D model of the tensegrity system is created by referencing dimensions from standard parts available at LS2N. The flanges are produced by 3D printing. With a standard universal coupling and three tension springs of stiffness k = 0.2 N/mm, the prototype is realized and it is depicted in the figure.

Figure 6 : A prototype of the tensegrity mechanism created using 3D printing and standard parts without cables

Analysis of the tensegrity mechanism

In the process of analysing the tensegrity structure firstly the vector coordinates of the base of the mechanism $B_1, B_2\ and\ B_3$ and the end-effector $C_1\ , C_2\ and\ C_3$ are figured out.

Calculation of Co-ordinates

The base frame is fixed i.e the side B. The spring mounting points on the fixed base are represented by B_i (i = 1, 2, 3) and they form the imaginary equilateral triangle of the manipulator base whose median is r_f for the 3-SPS-U mechanism.

$$b_i = R_{z(theta)n_i}$$

$$b_i = \begin{bmatrix} h * r_f \\ r_f * \sin\left(i * 2 * \frac{pi}{j}\right) \\ r_f * \cos\left(i * 2 * \frac{pi}{j}\right) \end{bmatrix} \quad For \quad i = 0,1,2$$

$$b_1 := \begin{bmatrix} h\ rf \\ 0 \\ rf \end{bmatrix}$$

$$b_2 := \begin{bmatrix} h\ rf \\ \frac{1}{2}\ rf\sqrt{3} \\ -\frac{1}{2}\ rf \end{bmatrix}$$

$$b_3 := \begin{bmatrix} h\,rf \\ -\frac{1}{2}\,rf\sqrt{3} \\ -\frac{1}{2}\,rf \end{bmatrix}$$

For estimating the vector co-ordinates of the end-effector mounting points, the XY Euler angle matrix is employed with respect to the central point A of the universal joint .The moving co-ordinate frame is the end-effector frame. The spring mounting points of the end-effector is represented by c_i (i = 1,2,3).

$$R = R_z(alpha) * R_y(\text{beta})$$

$$o_i = \begin{bmatrix} -h * r_f \\ r_f * \sin\left(i * 2 * \frac{pi}{j}\right) \\ r_f * \cos\left(i * 2 * \frac{pi}{j}\right) \end{bmatrix} \quad For\ i = 0,1,2.\ \ and\ \ j = 3$$

$$c_i = R * o_i$$

$$c_1 := \begin{bmatrix} -\cos(\alpha)\cos(\beta)\,h\,rf + \cos(\alpha)\sin(\beta)\,rf \\ -\sin(\alpha)\cos(\beta)\,h\,rf + \sin(\alpha)\sin(\beta)\,rf \\ -\sin(\beta)\,h\,rf + \cos(\beta)\,rf \end{bmatrix}$$

$$c_2 := \left[\left[-\cos(\alpha)\cos(\beta)\,h\,rf - \frac{1}{2}\sin(\alpha)\,rf\sqrt{3} - \frac{1}{2}\cos(\alpha)\sin(\beta)\,rf\right], \left[-\sin(\alpha)\cos(\beta)\,h\,rf + \frac{1}{2}\cos(\alpha)\,rf\sqrt{3} - \frac{1}{2}\sin(\alpha)\sin(\beta)\,rf\right], \left[-\sin(\beta)\,h\,rf - \frac{1}{2}\cos(\beta)\,rf\right]\right]$$

$$c_3 := \begin{bmatrix} \begin{bmatrix} -\cos(\alpha)\cos(\beta)\,h\,rf + \frac{1}{2}\sin(\alpha)\,rf\sqrt{3} \\ -\frac{1}{2}\cos(\alpha)\sin(\beta)\,rf \end{bmatrix}, \\ \begin{bmatrix} -\sin(\alpha)\cos(\beta)\,h\,rf - \frac{1}{2}\cos(\alpha)\,rf\sqrt{3} - \frac{1}{2}\sin(\alpha)\sin(\beta)\,rf \end{bmatrix}, \\ \begin{bmatrix} -\sin(\beta)\,h\,rf - \frac{1}{2}\cos(\beta)\,rf \end{bmatrix} \end{bmatrix}$$

R represents the spatial transformation matrix obtained from the Euler angles of universal joint and is used to identify the end-effector co-ordinate.

Calculation of length

The inverse geometric model for the mechanism is simpler and it is used to determine the length of springs between the base and end-effector at home-pose and working conditions. The equation is given by

$$l_i = \sqrt{(b_{ix} - c_{ix})^2 + \left(b_{iy} - c_{iy}\right)^2 + (b_{iz} - c_{iz})^2} \quad For\ \ i = 1,2,3$$

$$l_1 := \left(\left(h\,rf + \cos(\alpha)\cos(\beta)\,h\,rf - \cos(\alpha)\sin(\beta)\,rf\right)^2 + \left(\sin(\alpha)\cos(\beta)\,h\,rf - \sin(\alpha)\sin(\beta)\,rf\right)^2 + \left(rf + \sin(\beta)\,h\,rf - \cos(\beta)\,rf\right)^2 \right)^{1/2}$$

$$l_2 := \left(\left(h\,rf + \cos(\alpha)\cos(\beta)\,h\,rf + \frac{1}{2}\sin(\alpha)\,rf\sqrt{3} + \frac{1}{2}\cos(\alpha)\sin(\beta)\,rf \right)^2 + \left(\frac{1}{2}\,rf\sqrt{3} + \sin(\alpha)\cos(\beta)\,h\,rf - \frac{1}{2}\cos(\alpha)\,rf\sqrt{3} + \frac{1}{2}\sin(\alpha)\sin(\beta)\,rf \right)^2 + \left(-\frac{1}{2}\,rf + \sin(\beta)\,h\,rf + \frac{1}{2}\cos(\beta)\,rf \right)^2 \right)^{1/2}$$

$$l_3 := \left(\left(h\,rf + \cos(\alpha)\cos(\beta)\,h\,rf - \frac{1}{2}\sin(\alpha)\,rf\sqrt{3} + \frac{1}{2}\cos(\alpha)\sin(\beta)\,rf \right)^2 + \left(-\frac{1}{2}\,rf\sqrt{3} + \sin(\alpha)\cos(\beta)\,h\,rf + \frac{1}{2}\cos(\alpha)\,rf\sqrt{3} + \frac{1}{2}\sin(\alpha)\sin(\beta)\,rf \right)^2 + \left(-\frac{1}{2}\,rf + \sin(\beta)\,h\,rf + \frac{1}{2}\cos(\beta)\,rf \right)^2 \right)^{1/2}$$

Force vector

Tilting direction of the mechanism For an applied force, the tensegrity mechanism has to tilt along the direction of force. The position of β is identified where the mechanism tilts along the applied force. The 2D representation of the tensegrity mechanism will be used for calculations. The force vectors on can be calculated by the equation:

$$f_i = w * \frac{r_i}{norm(r_i)}$$

$$
\begin{aligned}
f1 := & \left[\left[\left(w \left(-\frac{1}{2} \sin(\alpha)\, rf\sqrt{3} - \frac{3}{2} \cos(\alpha) \sin(\beta)\, rf \right) \right) \Big/ \right. \right. \\
& \left(\left| \frac{1}{2} \sin(\alpha)\, rf\sqrt{3} + \frac{3}{2} \cos(\alpha) \sin(\beta)\, rf \right| + \left| \frac{1}{2} \cos(\alpha)\, rf\sqrt{3} \right. \right. \\
& \left. \left. - \frac{3}{2} \sin(\alpha) \sin(\beta)\, rf \right| + \frac{3}{2} \left| \cos(\beta)\, rf \right| \right) \Big], \\
& \left[\left(w \left(\frac{1}{2} \cos(\alpha)\, rf\sqrt{3} - \frac{3}{2} \sin(\alpha) \sin(\beta)\, rf \right) \right) \Big/ \right. \\
& \left(\left| \frac{1}{2} \sin(\alpha)\, rf\sqrt{3} + \frac{3}{2} \cos(\alpha) \sin(\beta)\, rf \right| + \left| \frac{1}{2} \cos(\alpha)\, rf\sqrt{3} \right. \right. \\
& \left. \left. - \frac{3}{2} \sin(\alpha) \sin(\beta)\, rf \right| + \frac{3}{2} \left| \cos(\beta)\, rf \right| \right) \Big], \\
& \left[-\frac{3}{2} \left(w \cos(\beta)\, rf \right) \Big/ \left(\left| \frac{1}{2} \sin(\alpha)\, rf\sqrt{3} \right. \right. \right. \\
& + \frac{3}{2} \cos(\alpha) \sin(\beta)\, rf \Big| + \left| \frac{1}{2} \cos(\alpha)\, rf\sqrt{3} \right. \\
& \left. \left. \left. - \frac{3}{2} \sin(\alpha) \sin(\beta)\, rf \right| + \frac{3}{2} \left| \cos(\beta)\, rf \right| \right) \right] \Big]
\end{aligned}
$$

$$
\begin{aligned}
f2 := & \left[\left[\left(w \left(\frac{1}{2} \sin(\alpha)\, rf\sqrt{3} - \frac{3}{2} \cos(\alpha) \sin(\beta)\, rf \right) \right) \Big/ \left(\left| \right. \right. \right. \right. \\
& \left. \left. \left. \left. -\frac{1}{2} \sin(\alpha)\, rf\sqrt{3} + \frac{3}{2} \cos(\alpha) \sin(\beta)\, rf \right| + \left| -\frac{1}{2} \cos(\alpha)\, rf\sqrt{3} \right. \right. \right. \right. \\
& \left. \left. \left. \left. - \frac{3}{2} \sin(\alpha) \sin(\beta)\, rf \right| + \frac{3}{2} \left| \cos(\beta)\, rf \right| \right) \right], \\
& \left[\left(w \left(-\frac{1}{2} \cos(\alpha)\, rf\sqrt{3} - \frac{3}{2} \sin(\alpha) \sin(\beta)\, rf \right) \right) \Big/ \left(\left| \right. \right. \right. \right. \\
& \left. \left. \left. \left. -\frac{1}{2} \sin(\alpha)\, rf\sqrt{3} + \frac{3}{2} \cos(\alpha) \sin(\beta)\, rf \right| + \left| -\frac{1}{2} \cos(\alpha)\, rf\sqrt{3} \right. \right. \right. \right. \\
& \left. \left. \left. \left. - \frac{3}{2} \sin(\alpha) \sin(\beta)\, rf \right| + \frac{3}{2} \left| \cos(\beta)\, rf \right| \right) \right], \\
& \left[-\frac{3}{2} \left(w \cos(\beta)\, rf \right) \Big/ \left(\left| -\frac{1}{2} \sin(\alpha)\, rf\sqrt{3} \right. \right. \right. \\
& + \frac{3}{2} \cos(\alpha) \sin(\beta)\, rf \Big| + \left| -\frac{1}{2} \cos(\alpha)\, rf\sqrt{3} \right. \\
& \left. \left. \left. - \frac{3}{2} \sin(\alpha) \sin(\beta)\, rf \right| + \frac{3}{2} \left| \cos(\beta)\, rf \right| \right) \right] \Big]
\end{aligned}
$$

Moments

There exist moments that are generated by the cables (mc) as well as the springs (ms) whose equations are given by:

Moments generated by cables mc is give as

$$mc = c_2 * f_1 + c_3 * f_2$$

$$ms = k * c_3 * f_2 + k * c_2 * f_1$$

$$m = mc + ms$$

Where k represents the stiffness of spring. We assume same stiffness for the three springs. The resultant moment m can be found by summing up the results of above equations. For attaining stable postures, the sum of components in the resultant moment m is equal to zero.

Static force analysis of the mechanism

With the inverse pendulum configuration being a suitable solution for the tensegrity mechanism, it is important to analyze its stability. In the case of pipelines with junctions, the active compliance has to be employed where the stability of tensegrity mechanism could be controlled through cables and the robot can be made to follow the right direction. For passive compliance, the cable actuation is not required and the objective of the mechanism will be to overcome the bend under passive mode. In this scenario, the static stability of the mechanism has to be determined and it should be capable of working passively without cable actuation.

According to Lagrange, for a moving system, the equation of motion is given by

$$\tau = \frac{d}{dt}\left(\frac{\partial T}{\partial q}\right) - \frac{\partial T}{\partial q} + \frac{dU}{dq} \qquad \text{where } q = [\alpha, \beta]^T$$

Potential energy

Under static conditions, the velocity of the system is zero and there exists no kinetic energies. The mass of the mechanism is also not taken into account as it vanishes along with the kinetic energy term. The potential energy of the system is contributed by the springs and cables. For this calculation, we assume the magnitudes of applied forces along the three cables as F1, F2, F3 and equal stiffness for the three springs as k. The total potential energy can be estimated by summing up the energies of springs and cables. The equations are given by:

$$U_{cable} = \sum_{i=1}^{3} F_i l_i \qquad U_{spring} = \sum_{i=1}^{3} \frac{1}{2} k l_i^2$$

$$U_{total} = U_{cable} + U_{spring}$$

Stability of the tensegrity mechanism

Under zero-applied forces or under the presence of a preload, the mechanism can deform due to the springs. The stability of mechanism has to be analyzed under static modes. For a tensegrity mechanism to be stable under static modes, the second order derivative or the stiffness of the mechanism K has to be positive. The Utot equation is first derived. Utot depends on the spring stiffness k, mounting radius r_f , parameter h. The stability of the system can be found by plotting the total potential energy against the alpha. The parameters k, r_f and h is considered as 0.2 N/mm, 11 mm and 1. The stability plot for the system is depicted in Figure

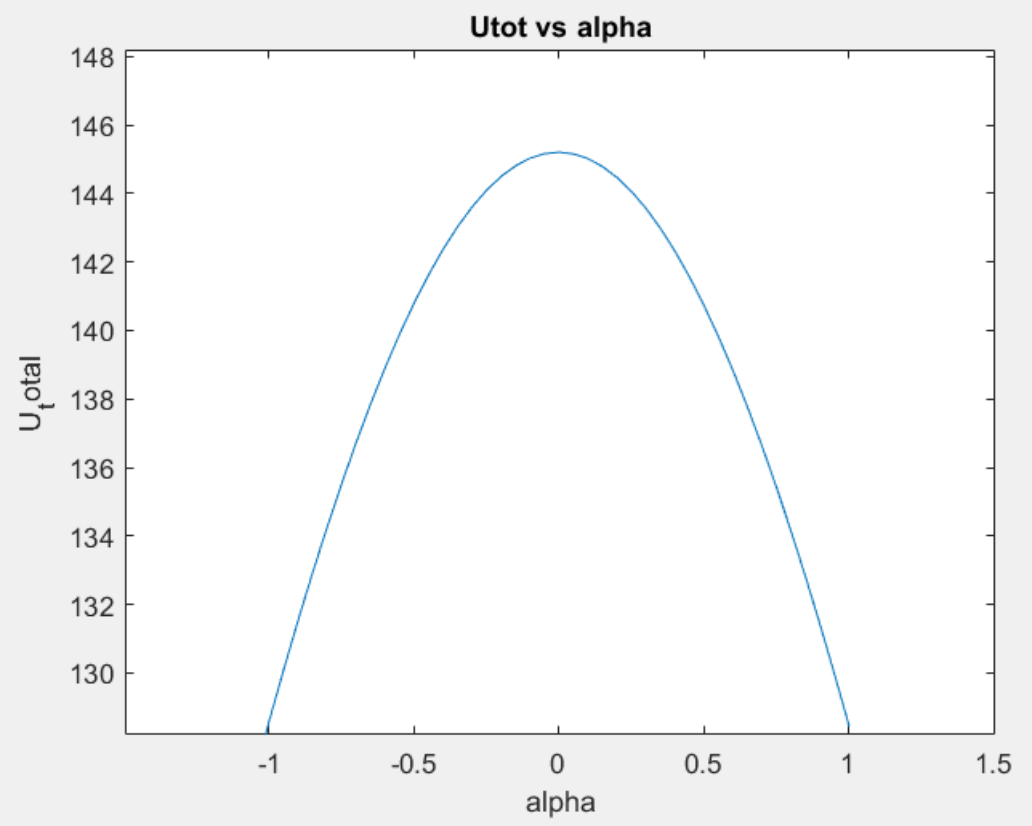

Figure 7 : Utotal vs alpha when h =1

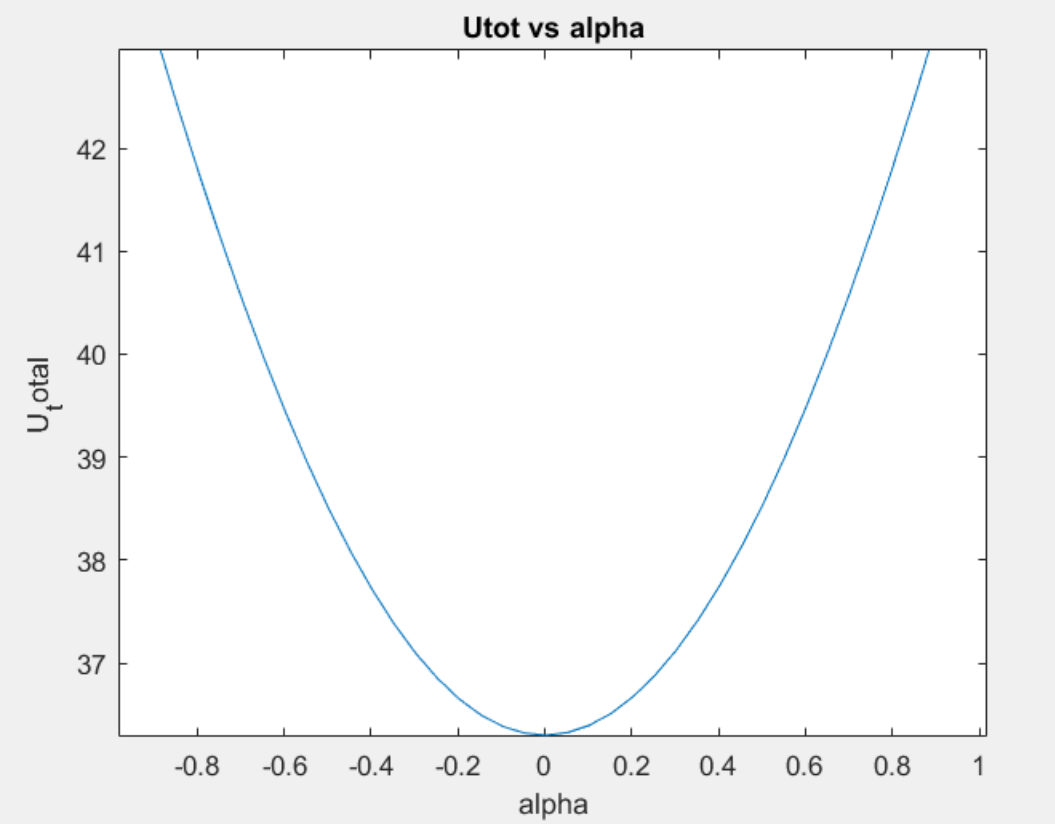

Figure 8 : Utotal vs alpha when h =0.5

It could be observed that the mechanism remains unstable and has maximum potential energy with no forces being applied. Under the influence of zero applied forces, the mechanism has no dependencies on the azimuth angle. Since Utot has a direct dependency on the applied forces, the system continues to remain unstable when the preload is considered. As observed from both the figures when the alpha is zero total potential energy reaches high values when the value of h is 1 and when h is 0.5 i.e, existing value from design then the total potential energy drops to lowest.

Mechanism stiffness

The second order derivative of Utot with respect to α which gives the mechanism stiffness K_α has to be studied for determining stable configuration. The applied forces are considered equal and are taken as F1 = F2 = F3 = F. The stiffness equation is generated using Maple with β & α at 0 radians and is given by:

$$K_\alpha = \frac{-3r_f(2kr_f h^2 + hF - kr_f)}{2}$$

It can be seen that the mechanism stiffness depends on the parameters r_f , h, F and k. By fixing one or several parameters, it is possible to determine a stable configuration. In this, we fix the

spring stiffness as per the prototype of 0.2 N/mm and a load of 2 N is considered for F. The stiffness K_α is then analyzed for varying values of h and r_f and their relations are shown below

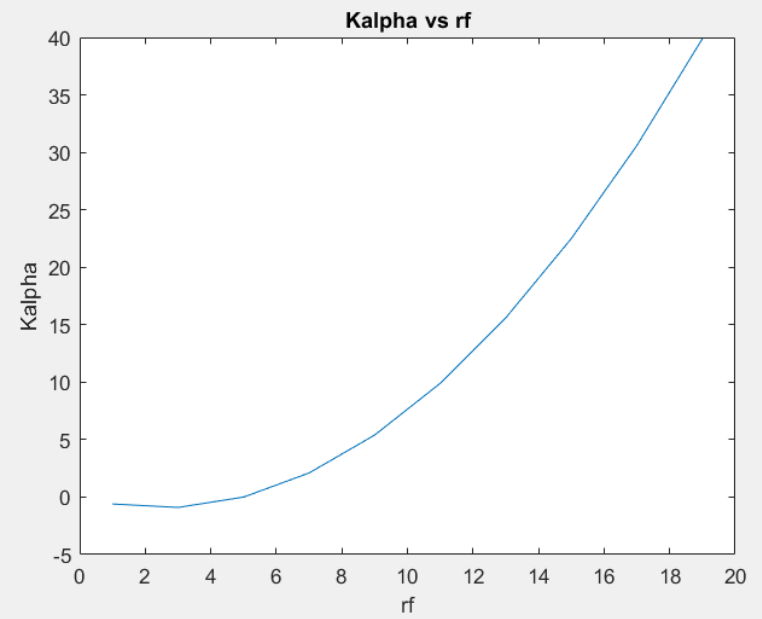

Figure 9 : Kalpha vs r_f

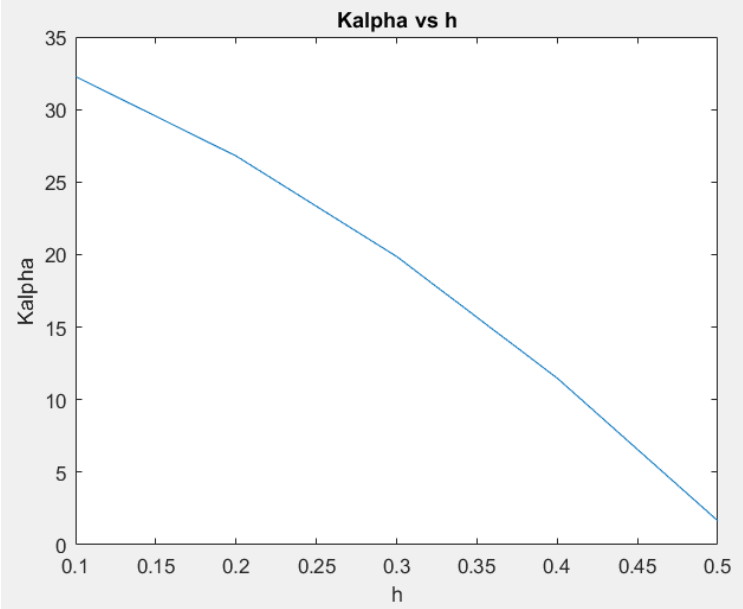

Figure 10 : Kalpha vs h

Acquired from the above graphs ,we can say that , K_α has a positive zone till the value of h reaches 0.5. As the parameter h increases more than 0.5, the negative zone of K_α is higher as shown in the above figures.. However, K_α transforms into negative values when r_f increases till 5 and when r_f increases from 5, K_α has a positive zone. By retaining r_f as 11 mm from the existing design of the robot, a value of h = 1/2 is chosen such that stiffness K_α is always positive with the preload.

Conclusion

The purpose of this project is to find the stability of the tensegrity in horizontal orientation. From the above results it can be said that with the static force analysis, this system was found to be unstable under zero applied forces. By fixing several parameters, the parameter h was modified to obtain a stable configuration under the presence of preload

Future works

The problems existing in the current design such as bending over 90 degrees can be overcome by stacking a second tensegrity module over the existing mechanism. Kinematics and workspace analysis was performed by Furet et al on stacked tensegrity system for 2D case. This problem will be extended for the 3D case because a stacked model can provide higher tilt angles. Also with stacked modules, it will be essential to check stability as there will be two tilt angles. In this case, the Hessian matrix will be derived and stability can be attained when the determinant of the Hessian matrix is always positive. The CATIA model of the robot with stacked tensegrity modules that resembles an “Elephant Trunk” is depicted in figure. Force analysis will further be extended on the stacked models assembled with the robot for various postures inside pipeline namely: vertical, horizontal and angled configurations for understanding the stability of the entire robot. An alternate approach will be proposed which deals with the study of variation of spring stiffness k and its impact on the mechanism stiffness K_α. An optimization technique will also be carried out for the determination of spring stiffness by taking into account the general design equations of a tension spring.

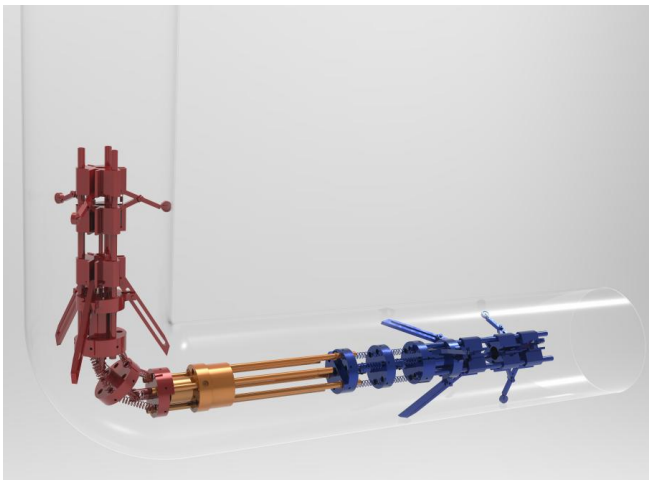

Figure 11 : Modified architecture of the robot with stacked tensegrity structures in CATIA

Code of MAPLE

```
> restart:
> with(LinearAlgebra):
> with(plots):
> #Note
#IN ORDER TO GET GRAPHS OF
#FOR ut ONLY alpha IS COMMENTED
#FOR kalpha VS rf,rf SHOULD BE COMMENTED
#FOR kalpha VS h,h SHOULD BE COMMENTED
>
Rotx(theta):= Matrix([[1,0,0],[0,cos(theta),-
sin(theta)],[0,sin(theta),cos(theta)]]):
Rotz(alpha):= Matrix([[cos(alpha),-
sin(alpha),0],[sin(alpha),cos(alpha),0],[0,0,1]]):
Roty(beta):=
Matrix([[cos(beta),0,sin(beta)],[0,1,0],[sin(beta),0,cos(beta)]]
):
> R := Rotz(alpha).Roty(beta):
j:=3:
for i from 0 to 2 by 1
do
o[i+1]:= Vector([-h*rf, rf*sin(i*2*Pi/j),rf*cos(i*2*Pi/j)]):
c[i+1]:= R.o[i+1];
cx[i+1] := c[i+1][1];
cy[i+1] := c[i+1][2];
cz[i+1] := c[i+1][3];
b[i+1]:= Vector([h*rf, rf*sin(i*2*Pi/j),rf*cos(i*2*Pi/j)]):
bbx[i+1] := b[i+1][1];
bby[i+1] := b[i+1][2];
bbz[i+1] := b[i+1][3];
end do:
>
for i from 1 to 3 by 1
do
l[i]:=sqrt(((bbx[i]-cx[i])^2)+((bby[i]-cy[i])^2)+((bbz[i]-
cz[i])^2));
end do:
>
r1 := c[2]-c[1]:
r2 := c[3]-c[1]:
z1 := norm(r1,1):
z2 := norm(r2,1):
f1 := w*r1/z1:
f2 := w*r2/z2:
>
#h:=1;
#k:=0.2;
```

```
#alpha:=0;
#beta := Pi/2;
#rf:=10;

mc := c[2].f1+c[3].f2:
ms := k*c[3].f2+k*c[2].f1:
m := mc+ms:
> #alpha:=0:
beta := 0:
k := 0.2:
h := 1:
rf := 10:
i:=1:
F[i]:= 0:
F[i+1]:=0:
F[i+2]:=0:
uc:= F[i]*l[i]+F[i+1]*l[i+1]+F[i+2]*l[i+2]:
us := 0.5*k*(l[i]*l[i]+l[i+1]*l[i+1]+l[i+2]*l[i+2]):
ut := uc+us:
plot(ut,alpha=-Pi/6..Pi/6):
> kalpha := diff(ut,alpha):
>
K := diff(kalpha,alpha):
> #alpha:=0:
beta := 0:
k := 0.2:
#h := 1:
rf := 10:
#G:= K;
#plot(K,rf=20..1);
#plot(K,h=0..1);
```